

Impaired response of hypoxic sensor protein HIF-1 α and its downstream proteins in the spinal motor neurons of ALS model mice

Kota Sato, Nobutoshi Morimoto, Tomoko Kurata, Takafumi Mimoto, Kazunori Miyazaki, Yoshio Ikeda,
and Koji Abe*

Department of Neurology, Okayama University Graduate School of Medicine, Dentistry and
Pharmaceutical Sciences, Okayama, Japan

*Correspondence to Professor Koji Abe, Department of Neurology, Okayama University Graduate
School of Medicine and Dentistry, 2-5-1 Shikata-cho, Okayama 700-8558, Japan.

Tel: +81-86-235-7365, Fax: +81-86-235-7368

E-mail: kosatou@cc.okayama-u.ac.jp

Running Header: HIF-1 α and its downstream proteins in ALS model mice

INTRODUCTION

Amyotrophic lateral sclerosis (ALS) is a progressive and fatal disease caused by the selective death of motor neurons. Approximately 5–10% of patients have a genetically inherited form known as familial ALS (FALS). Approximately 15–20% of FALS cases are associated with missense mutations or small deletions in the gene that encodes SOD1 (Aoki et al., 1993; Rosen et al., 1993). Transgenic (Tg) mice that carry mutant SOD1 genes provided an animal model that has helped elucidate how mutations in the SOD1 gene cause motor neuron death (Gurney et al., 1994; Murakami et al., 2007). Although the underlying mechanism of ALS has not yet been fully clarified, several reports have implicated the involvement of oxidative stress in the selective death of motor neurons in both ALS patients and animal models (Abe, 2007; Barber and Shaw, 2010; Barnham et al., 2004; Miyazaki et al., 2009; Robberecht, 2000; Warita et al., 2001).

We previously showed blood flow-metabolism uncoupling in the affected spinal cords from the pre-symptomatic stage ALS model mice, suggesting relative spinal cord hypoxia (Miyazaki et al., 2011a). We also showed a selective lack of vascular endothelial growth factor (VEGF) induction in motor neurons (MNs) after hypoxic exposure in SOD1-Tg ALS model mice (Ilieva et al., 2003; Murakami et al., 2003). Other studies have suggested that the lack of VEGF induction is linked to the degeneration of

motor neurons in ALS (Cleveland and Rothstein, 2001; Ischiropoulos and Beckman, 2003; Lambrechts et al., 2003). Under hypoxic conditions, VEGF is activated by hypoxia inducible factor (HIF-1), which consists of a heterodimer of two basic helix-loop-helix PAS (Per-ARNT-Sim) proteins, HIF-1 α and HIF-1 β . HIF-1 α accumulates in response to hypoxia, whereas HIF-1 β is constitutively expressed. Thus, HIF1- α serves as an important mediator of the hypoxic response and upregulates important angiogenic factors, such as VEGF and VEGF receptor 1 (Sharp and Bernaudin, 2004). While HIF-1 α expression is increased in the spinal cord of ALS model mice (Xu et al., 2011), the combination of HIF-1 α and downstream proteins, such as heme oxygenase-1 (HO-1) and erythropoietin (EPO), as well as VEGF, have not been studied in ALS.

In the present study, we examined temporal and spatial changes in HIF-1 α , VEGF, HO-1, and EPO over the course of motor neuron degeneration in the spinal cord of ALS model mice.

RESULTS

Immunohistochemical analyses of hypoxic sensor proteins HIF-1 α , VEGF, HO-1, and EPO

Nissl staining showed no change in the number of large motor neurons (MNs) in the lumbar spinal anterior horn at 10, 14 and 18W in WT mice (Fig. 1 Aa). Tg mice showed a progressive loss of large MNs from 14 to 18W (Fig. 1 Ac, d), with a progressive increase in the number of surrounding small glial cells (Fig. 1 A, c, d).

In the spinal cord of WT mice, HIF-1 α was slightly detected in the cytoplasm of anterior large MNs and surrounding small glial cells at 10-18W (Fig. 1 Ae). In Tg mice, HIF-1 α staining strength and intracellular localization progressively accumulated in the MNs of Tg mice, especially at 18W (Fig. 1 Af-h, arrowheads). HIF-1 α staining in the surrounding glial cells of Tg mice also progressively accumulated at 18W (Fig. 1 Ag-h, arrows).

VEGF immunoreactivity was slightly detected in both the cytoplasm of anterior large MNs and surrounding small glial cells in WT mice at 10-18W (Fig. 1 Ai). In the spinal cord of Tg mice, VEGF staining strength and intracellular localization did not change in large MNs at 10-18W (Fig. 1 Aj-l, arrowheads), but VEGF staining progressively accumulated in the surrounding glial cells of Tg mice,

especially at 18W (Fig. 1 Ak-l, arrows).

HO-1 immunoreactivity was also detected in the cytoplasm of anterior large MNs and surrounding small glial cells in WT mice at 10-18W (Fig. 1 Am). In the spinal cord of Tg mice, HO-1 staining strength and intracellular localization did not change in MNs at 10-18W (Fig. 1 An-p, arrowheads), whereas it progressively accumulated in the surrounding glial cells of Tg mice, especially at 18W (Fig. 1 Ap, arrows).

Finally, EPO immunoreactivity was detected mainly in the cytoplasm of anterior large MNs and surrounding small glial cells in WT mice at 10-18W (Fig. 1 Am). In the spinal cord of Tg mice, EPO staining strength and intracellular localization did not change in MNs at 10-18W (Fig. 1 A, q-s, arrowheads). In contrast, the ratio of EPO-positive glia-like cells was decreased, especially at 18W (Fig. 1 At, arrows).

Accounting for the different number of anterior large MNs and glia-like cells, the relative ratios of the number of VEGF-, HO-1-, and EPO-positive to Nissl-stained cells showed no significant changes at 10-14W in large MNs (Fig. 1 Bv-1, w-1, x-1); only HIF-1 α showed a significant increase at 18W in Tg mice (0.55 ± 0.10 , $**p < 0.01$ vs. WT, $###p < 0.01$ vs. 10W Tg, Fig. 1 Bu-1). In contrast, the relative ratio of the number of HIF-1 α -positive to Nissl-stained surrounding glial cells was significantly

increased at 14W (0.51 ± 0.06 , $*p < 0.05$ vs. WT, $\#p < 0.05$ vs. 10W Tg, Fig. 1 Bu-2) and 18W in Tg mice (0.74 ± 0.03 , $**p < 0.01$ vs. WT, $###p < 0.01$ vs. 10W Tg, Fig. 1 Bu-2). The ratio of VEGF positive surrounding glial cells was significantly increased at 18W in Tg mice (0.69 ± 0.04 , $*p < 0.05$ vs. WT, $\#p < 0.05$ vs. 10W Tg, Fig. 1 Bv-2), as was the ratio of HO-1-positive surrounding glial cells at 14W (0.65 ± 0.08 , $*p < 0.05$ vs. WT, Fig. 1 Bw-2) and 18W in Tg mice (0.82 ± 0.09 , $*p < 0.05$ vs. WT, $\#p < 0.05$ vs. 10W Tg, Fig. 1 Bw-2). In contrast, the ratio of EPO-positive glial cells significantly reduced at 18W of Tg mice (0.35 ± 0.04 , $*p < 0.05$ vs. WT, Fig. 1 Bx-2).

Double immunofluorescence analysis

In the spinal cord of WT mice, HIF-1 α was detected mainly in the cytoplasm of anterior large MNs (Fig. 2 A, WT, red). In the spinal cord of Tg mice, the intracellular localization of HIF-1 α did not change at 10-18W in anterior large MNs (Fig. 2 A, Tg, red). HIF-1 α plus neurofilament double-positive cells were found both in WT and 10-18W Tg in large MNs (Fig. 2 A, bottom).

In astroglial cells, HIF-1 α plus GFAP double-positive cells were not detected in the spinal cord of WT mice (Fig. 2 B, WT, Merge). In the Tg mice, HIF-1 α plus GFAP double-positive cells showed a progressively increased intensity at 10-18W in Tg mice (Fig. 2 B, bottom).

In microglial cells, HIF-1 α plus Iba-1 double-positive cells were not detected in the spinal cord of WT mice (Fig. 2 C, WT, Merge), whereas HIF-1 α plus Iba-1 double-positive cells became evident at 14-18W in the spinal cord of Tg mice (Fig. 2 C, bottom).

Western blot analyses of hypoxic sensor proteins HIF-1 α , VEGF, HO-1, and EPO

Western blot analysis showed that HIF-1 α protein levels in WT mice did not change significantly with age at 10-18W (Fig. 3, white bars), but Tg mice showed a progressive increase in the HIF-1 α protein ratio relative to β -tubulin: 0.19 ± 0.06 at 10W (Fig. 3, gray bar), 0.28 ± 0.02 at 14W ($*p < 0.05$ vs. 14W WT, Fig. 3, dark bar), and 0.49 ± 0.06 at 18 W ($**p < 0.01$ vs. 18W WT, $##p < 0.01$ vs. 10W Tg, $\$p < 0.05$ vs. 14W Tg, Fig. 3, black bar).

VEGF protein levels in WT mice did not change significantly with age at 10-18W by Western blot analysis (Fig. 4, white bars). Tg mice also did not show any significant change in VEGF protein levels relative to β -tubulin: 0.41 ± 0.05 at 10W, 0.41 ± 0.06 at 14W, and 0.50 ± 0.08 at 18 W (Fig. 4, gray, dark, and black bars).

The third Western blot analysis showed that HO-1 protein levels in WT mice did not change significantly with age at 10-18W (Fig. 5, white bars). However, Tg mice showed a remarkable increase in

HO-1 protein levels relative to β -tubulin at 18W: 0.36 ± 0.07 (** $p < 0.01$ vs. 18W WT, ## $p < 0.01$ vs. 10W Tg, Fig. 5, black bars) compared to 0.11 ± 0.02 at 10W, 0.12 ± 0.02 at 14W.

The fourth Western blot analysis showed that EPO protein levels in WT mice did not change significantly with age at 10-18W (Fig. 6, white bars). Tg mice also did not show any significant change in protein levels relative to β -tubulin: 0.99 ± 0.15 at 10W, 0.82 ± 0.10 at 14W, and 0.82 ± 0.12 at 18 W (Fig. 6, gray, dark, and black bars).

DISCUSSION

The present study investigated the presence of and changes to hypoxic stress sensor proteins regulated by the protein HIF-1 α in the lumbar anterior horn of ALS model mice. The results demonstrated progressive increases in HIF-1 α protein expression both in the anterior large MNs and surrounding glial cells in Tg mice from 14W, with significant breaks in the glial cells between early symptomatic 14W and end stage 18W (Fig. 1 Ag-h, Bu, and Fig. 3). Double immunofluorescence analyses revealed that HIF-1 α plus GFAP and Iba-1 double-positive surrounding glial cells showed progressively increased intensity at 10-18W (Fig. 2 B, C). Expression of VEGF and HO-1 also showed a progressive increase but were significant only in the surrounding glial cells at 18W (Fig. 1 Aj-l, n-p, Bv, w); however, Western blot analyses only showed a significant increase at 18W in HO-1 but not VEGF (Fig. 4, 5). In contrast, EPO protein expression was decreased in the surrounding glial cells of Tg mice at 18W (Fig. 1 At, Bx-2). This is the first report demonstrating the induction of the hypoxic stress sensor protein HIF-1 α with downstream protein expression alterations in VEGF, HO-1 and EPO.

We recently demonstrated that ALS model mice possessed a damaged oxidative stress sensor system with Kelch-like ECH-associated protein 1 (Keap1)/nuclear erythroid 2-related factor 2 (Nrf2) expressed in the anterior large MNs (Mimoto et al., 2012). Another report showed the activation of Nrf2

in spinal cord motor neurons in ALS model mice when protected by ethylamine (Neymotin et al., 2011).

Our previous reports that showed the selective lack of vascular endothelial growth factor (VEGF) induction in MNs after hypoxic exposure in ALS model mice (Ilieva et al., 2003; Murakami et al., 2003), as well as other studies of chronic hypoxia (Cleveland and Rothstein, 2001; Ischiropoulos and Beckman, 2003; Lambrechts et al., 2003). All of these findings indicate that both oxidative and hypoxic stresses may be important pathogenic mechanisms in ALS.

Hypoxia triggers a series of alterations in neuronal events, such as membrane dysfunction and depolarization, metabolic decline, signal transduction deficiency, and abnormal cell morphology (Chao and Xia, 2010); it also affects the expression of hypoxic stress sensor proteins. HIF-1 plays a central role in cellular adaptation to hypoxia by transcriptionally upregulating its target genes, which are involved in angiogenesis, erythropoiesis, and glycolysis, in addition to other processes (Tanaka and Nangaku, 2009). HIF-1 consists of α and β subunits and mainly exists as a heterodimer with multiple effects (Ebert et al., 1995), including dilatation of blood vessels by inducing nitric oxide synthetase and HO-1 (Semenza, 1998) and promotion of angiogenesis via VEGF induction (Ebert et al., 1995). We have shown blood flow-metabolism uncoupling and decreased spinal blood flow in the affected spinal anterior gray matter from the pre-symptomatic stage in these mice. We suggested that this early and progressive

flow-metabolism uncoupling could be profoundly involved in the entire disease process as a vascular component of ALS pathology, suggesting a relative hypoxia in the spinal cord (Miyazaki et al., 2011a).

In our previous study, HIF-1 α was strongly induced in the ischemic core and penumbra with a peak at 2 hours after transient middle cerebral artery occlusion (Zhang et al., 2010). The present study demonstrated a progressive increase in HIF-1 α protein expression both in the anterior large MNs and surrounding glial cells of Tg mice from 14 to 18W (Fig. 1 Ag-h, Bu, and Fig. 3). HO-1 and VEGF were also increased in the surrounding glial cells of Tg mice at 18W (Fig. 1 Aj-l, n-p, Bv-2, w-2). Conversely, EPO was significantly decreased in the surrounding glial cells of Tg mice at 18W (Fig. 1 At, Bx-2). These findings support previous studies showing the increase of HIF-1 α (Xu et al., 2011) and VEGF (Murakami et al., 2003) protein levels in G93A Tg mice. However, the time point of VEGF protein increase was late compared to that of HIF-1. A previous study showed VEGF mRNA was down-regulated in the spinal cord of G93A Tg mice, and in the glial cells expressing mutant SOD1 (Lu et al., 2007). The temporal difference of HIF-1 and VEGF protein increase could be partly explained by VEGF dysregulation by the mutant SOD1. Several studies mentioned that exogenous VEGF was neuroprotective by activation of VEGF receptor and subsequent Akt signaling (Lunn et al., 2009; Zheng et al., 2004; Zheng et al., 2007). Therefore, the dysregulation of VEGF in the spinal cord of ALS mice

might be related to ALS progression. The HO-1 increase of Tg mice (Fig. 1 Bw-2) may also be related to Nrf2, because Nrf/antioxidant response element (ARE) pathway also regulates HO-1 protein levels (Mimoto et al., 2012). During hypoxia, EPO reduced neuronal cell death with glucose deprivation (Sinor and Greenberg, 2000). In the present study, however, EPO was not increased in the anterior large MNs of Tg mice but was decreased in the surrounding glial cells. A previous study also showed that EPO expression was increased not in the anterior horn but in unaffected areas including the brainstem nuclei of ALS model mice (Chung et al., 2004). A recent study demonstrated that the EPO level in cerebrospinal fluid was lower in ALS patients than in other neurodegenerative patients (Brettschneider et al., 2006).

In summary, we found that the hypoxic sensor protein HIF-1 α was induced more in the surrounding glial cells than in the most affected anterior large MNs. In addition, downstream proteins responded only in the surrounding glial cells at the late to end stages of ALS progression. These findings indicate that MNs profoundly lack the neuro-protective response of the HIF-1 α system to hypoxic stress, which could be an important mechanism of neurodegeneration in ALS.

MATERIALS AND METHODS

Animal Model

All experimental procedures were carried out according to the guidelines of the Animal Care and Use Committee of the Graduate School of Medicine, Dentistry, and Pharmaceutical Science of Okayama University. A Transgenic (Tg) mouse line with the G93A human SOD1 mutation (G1H/1) was obtained from Jackson Laboratories (Bar Harbor, ME) and maintained as hemizygotes by mating Tg males with C57BL/6J females. The offspring were genotyped using a PCR assay with DNA obtained from tail tissue samples according to our previous methods (Miyazaki et al., 2011b; Morimoto et al., 2009). G93A Tg mice show disease onset at roughly 14 weeks (W) of age and die approximately 3-4 weeks later. Thus, we took 10, 14, and 18 W G93A male mice for the presymptomatic stage, early symptomatic stage, and end stage, respectively. We used age-matched non-Tg C57BL/6J male littermates (WT) as controls.

Primary Antibodies

For immunohistochemistry and/or Western blot analysis, the following primary antibodies were used: mouse anti-HIF-1 α monoclonal antibody (Novus Biologicals, CO, USA), rabbit anti-VEGF polyclonal antibody (Abcam, MA, USA), rabbit anti-HO-1 polyclonal antibody (Enzo Life Science, NY, USA), rabbit anti-EPO polyclonal antibody (Santa Cruz, CA, USA), rabbit anti neurofilament polyclonal

antibody (Millipore, MA, USA), goat anti-GFAP monoclonal antibody (Millipore, MA, USA), goat anti-Iba-1 polyclonal antibody (Abcam, Cambridge, MA), and mouse anti- β -tubulin monoclonal antibody (Sigma, Tokyo, Japan).

Immunohistochemical Analysis

At 10, 14 or 18 W (n = 5 each), each mouse was deeply anesthetized with pentobarbital (40 mg/kg, i.p.) and transcardially perfused with heparinized saline followed by 4 % paraformaldehyde in 0.1 M phosphate buffer (pH 7.4). The lumbar spinal cord spanning L4-5 was removed and further fixed by immersion in the same fixative for 4 h and then frozen after cryoprotection with a series of phosphate-buffered sucrose solutions of increasing concentration (10, 20, and 30 %). Transverse sections of 10 μ m thickness were cut through the lumbar cord on a cryostat. The sections were first incubated in 0.3 % H₂O₂/methanol for 10 min to block endogenous peroxidase activity. The sections were then incubated with primary antibodies overnight at 4°C. After being washed in phosphate-buffered saline (PBS, pH 7.4), the sections were incubated with the appropriate biotinylated IgG (1:500; Invitrogen, Eugene, OR) for 1 h at room temperature. After being washed in PBS, the sections were incubated with ABC complex (Vector Laboratories, Burlingame, CA) for 30 min at room temperature and then

visualized with 3,3'-diaminobenzidine tetrahydrochloride (DAB). To confirm the specificity of the primary antibody, a set of sections was stained in a similar manner but without the primary antibodies. The dilutions of primary antibodies in this study were as follows: anti-HIF-1 α (1:500), VEGF (1:200), HO-1 (1:200), and EPO (1:100).

Cell Quantification

For quantitative analysis, the sections from the same animal with immunohistochemical analysis were also stained with cresyl violet staining (Nissl stain), and all cells in the ventral horns, below a lateral line across the spinal cord from the central canal, were microscopically video-captured. The cells with a diameter greater than 20 μ m with a clear nucleoli were quantified as anterior large MNs as described previously (Ohta et al., 2006), and the cells without Nissl were quantified as surrounding glial cells in the same manner. The immunopositive cells were compared with Nissl stain (large MNs and the surrounding glial cells, respectively).

Double immunofluorescence analysis

To determine the detailed spatial distribution of each protein, 10 μ m lumbar sections were

incubated with a mixture of anti-HIF-1 α (1:500) plus neurofilament (1:500), GFAP (1:500), or Iba-1 (1:500) overnight at 4°C. After being rinsed in PBS, the sections were simultaneously incubated with two appropriate Alexa fluor-conjugated secondary antibodies (1:500; Invitro-gen) for 1 hr at room temperature. The sections were scanned using a confocal microscope equipped with argon and HeNe1 lasers (LSM-510; Zeiss, Jena, Germany).

Western blot analysis

With each set of animals (n = 5 each), each mouse at 10, 14 or 18 W was deeply anesthetized with pentobarbital (40 mg/kg, i.p.) and decapitated. The lumbar spinal cord was removed. The lumbar cord samples were sonicated in ice-cold lysis buffer containing 50 mM Tris-HCl (pH 7.2), 250 mM NaCl, 1 % NP-40, and Complete Mini Protease Inhibitor Cocktail (Roche, Basel, Switzerland). The lysate was centrifuged at 12,000 g for 10 min at 4°C, the supernatant was collected, and the protein concentration was determined by the Lowry assay (Bio-Rad, Hercules, CA, USA). Twenty micrograms of the total protein extract was loaded onto a 12.5 % polyacrylamide gel, separated by sodium dodecyl sulfate (SDS)-polyacrylamide gel electrophoresis, and transferred to a polyvinylidene fluoride membrane (Millipore, MA, USA). After being washed with PBS containing 5 % skim milk and 0.2 % Tween 20, the

membranes were incubated with primary antibody overnight at 4°C. After being washed with PBS, the membranes were probed with an appropriate horseradish peroxidase-conjugated secondary antibody (Amersham Biosciences, Buckinghamshire, UK), and immunodetection was performed with an enhanced chemiluminescent substrate (Pierce, Rockford, IL). After the ECL detection, the membranes were incubated in stripping buffer (62.5 mM Tris-HCl, pH 6.7; 2 % SDS; 0.7 % β -mercaptoethanol) at 50°C for 15 min and then re-probed with a monoclonal anti- β -tubulin antibody (1:5,000; Sigma, Tokyo, Japan) as a loading control for protein quantification. The signals were quantified with a luminoimage analyzer (LAS 1000-Mini; Fuji Film, Tokyo, Japan), and quantitative densitometric analysis was performed using Image J software. The dilutions of primary antibodies in this study were as follows: anti-HIF-1 α (1:1,000), VEGF (1:1,000), HO-1 (1:1,000), EPO (1:1,000), β -tubulin (1:5,000)

Statistical Analysis

Significant differences in the Western blot and immunohistochemical analyses with DAB staining between the age-matched WT and Tg mice were evaluated using Welch's t-test. Statistical significance was accepted at $p < 0.05$.

ACKNOWLEDGMENTS

This work was partly supported by the Grant-in-Aid for Scientific Research (B) 21390267 and the Ministry of Education, Science, Culture and Sports of Japan, Grants-in-Aid from the Research Committee of CNS Degenerative Diseases (Nakano I), and grants (Mizusawa H, Nishizawa M, Sasaki H) from the Ministry of Health, Labor and Welfare of Japan.

REFERENCES

- Abe, K., 2007. [Pathogenesis and therapeutic perspectives for amyotrophic lateral sclerosis (ALS)]. *Rinsho Shinkeigaku*. 47, 790-4.
- Aoki, M., Ogasawara, M., Matsubara, Y., Narisawa, K., Nakamura, S., Itoyama, Y., Abe, K., 1993. Mild ALS in Japan associated with novel SOD mutation. *Nat Genet*. 5, 323-4.
- Barber, S.C., Shaw, P.J., 2010. Oxidative stress in ALS: key role in motor neuron injury and therapeutic target. *Free Radic Biol Med*. 48, 629-41.
- Barnham, K.J., Masters, C.L., Bush, A.I., 2004. Neurodegenerative diseases and oxidative stress. *Nat Rev Drug Discov*. 3, 205-14.
- Brettschneider, J., Widl, K., Ehrenreich, H., Riepe, M., Tumani, H., 2006. Erythropoietin in the cerebrospinal fluid in neurodegenerative diseases. *Neurosci Lett*. 404, 347-51.
- Chao, D., Xia, Y., 2010. Ionic storm in hypoxic/ischemic stress: can opioid receptors subside it? *Prog Neurobiol*. 90, 439-70.
- Chung, Y.H., Joo, K.M., Kim, Y.S., Lee, K.H., Lee, W.B., Cha, C.I., 2004. Enhanced expression of erythropoietin in the central nervous system of SOD1(G93A) transgenic mice. *Brain Res*. 1016, 272-80.

- Cleveland, D.W., Rothstein, J.D., 2001. From Charcot to Lou Gehrig: deciphering selective motor neuron death in ALS. *Nat Rev Neurosci.* 2, 806-19.
- Ebert, B.L., Firth, J.D., Ratcliffe, P.J., 1995. Hypoxia and mitochondrial inhibitors regulate expression of glucose transporter-1 via distinct Cis-acting sequences. *J Biol Chem.* 270, 29083-9.
- Gurney, M.E., Pu, H., Chiu, A.Y., Dal Canto, M.C., Polchow, C.Y., Alexander, D.D., Caliendo, J., Hentati, A., Kwon, Y.W., Deng, H.X., et al., 1994. Motor neuron degeneration in mice that express a human Cu,Zn superoxide dismutase mutation. *Science.* 264, 1772-5.
- Ilieva, H., Nagano, I., Murakami, T., Shiote, M., Shoji, M., Abe, K., 2003. Sustained induction of survival p-AKT and p-ERK signals after transient hypoxia in mice spinal cord with G93A mutant human SOD1 protein. *J Neurol Sci.* 215, 57-62.
- Ischiropoulos, H., Beckman, J.S., 2003. Oxidative stress and nitration in neurodegeneration: cause, effect, or association? *J Clin Invest.* 111, 163-9.
- Lambrechts, D., Storkebaum, E., Morimoto, M., Del-Favero, J., Desmet, F., Marklund, S.L., Wyns, S., Thijs, V., Andersson, J., van Marion, I., Al-Chalabi, A., Bornes, S., Musson, R., Hansen, V., Beckman, L., Adolfsson, R., Pall, H.S., Prats, H., Vermeire, S., Rutgeerts, P., Katayama, S., Awata, T., Leigh, N., Lang-Lazdunski, L., Dewerchin, M., Shaw, C., Moons, L., Vlietinck, R., Morrison, K.E., Robberecht, W., Van Broeckhoven, C., Collen, D., Andersen, P.M., Carmeliet, P., 2003. VEGF is a modifier of amyotrophic lateral sclerosis in mice and humans and protects motoneurons against ischemic death. *Nat Genet.* 34, 383-94.
- Lu, L., Zheng, L., Viera, L., Suswam, E., Li, Y., Li, X., Estevez, A.G., King, P.H., 2007. Mutant Cu/Zn-superoxide dismutase associated with amyotrophic lateral sclerosis destabilizes vascular endothelial growth factor mRNA and downregulates its expression. *J Neurosci.* 27, 7929-38.
- Lunn, J.S., Sakowski, S.A., Kim, B., Rosenberg, A.A., Feldman, E.L., 2009. Vascular endothelial growth factor prevents G93A-SOD1-induced motor neuron degeneration. *Dev Neurobiol.* 69, 871-84.
- Mimoto, T., Miyazaki, K., Morimoto, N., Kurata, T., Satoh, K., Ikeda, Y., Abe, K., 2012. Impaired antioxidative Keap1/Nrf2 system and the downstream stress protein responses in the motor neuron of ALS model mice. *Brain Res.*
- Miyazaki, K., Nagai, M., Morimoto, N., Kurata, T., Takehisa, Y., Ikeda, Y., Abe, K., 2009.

- Spinal anterior horn has the capacity to self-regenerate in amyotrophic lateral sclerosis model mice. *J Neurosci Res.* 87, 3639-48.
- Miyazaki, K., Masamoto, K., Morimoto, N., Kurata, T., Mimoto, T., Obata, T., Kanno, I., Abe, K., 2011a. Early and progressive impairment of spinal blood flow-glucose metabolism coupling in motor neuron degeneration of ALS model mice. *J Cereb Blood Flow Metab.*
- Miyazaki, K., Ohta, Y., Nagai, M., Morimoto, N., Kurata, T., Takehisa, Y., Ikeda, Y., Matsuura, T., Abe, K., 2011b. Disruption of neurovascular unit prior to motor neuron degeneration in amyotrophic lateral sclerosis. *J Neurosci Res.* 89, 718-28.
- Morimoto, N., Nagai, M., Miyazaki, K., Kurata, T., Takehisa, Y., Ikeda, Y., Kamiya, T., Okazawa, H., Abe, K., 2009. Progressive decrease in the level of YAP Δ Cs, prosurvival isoforms of YAP, in the spinal cord of transgenic mouse carrying a mutant SOD1 gene. *J Neurosci Res.* 87, 928-36.
- Murakami, T., Ilieva, H., Shiote, M., Nagata, T., Nagano, I., Shoji, M., Abe, K., 2003. Hypoxic induction of vascular endothelial growth factor is selectively impaired in mice carrying the mutant SOD1 gene. *Brain Res.* 989, 231-7.
- Murakami, T., Nagai, M., Miyazaki, K., Morimoto, N., Ohta, Y., Kurata, T., Takehisa, Y., Kamiya, T., Abe, K., 2007. Early decrease of mitochondrial DNA repair enzymes in spinal motor neurons of presymptomatic transgenic mice carrying a mutant SOD1 gene. *Brain Res.* 1150, 182-9.
- Neymotin, A., Calingasan, N.Y., Wille, E., Naseri, N., Petri, S., Damiano, M., Liby, K.T., Risingsong, R., Sporn, M., Beal, M.F., Kiaei, M., 2011. Neuroprotective effect of Nrf2/ARE activators, CDDO ethylamide and CDDO trifluoroethylamide, in a mouse model of amyotrophic lateral sclerosis. *Free Radic Biol Med.* 51, 88-96.
- Ohta, Y., Nagai, M., Nagata, T., Murakami, T., Nagano, I., Narai, H., Kurata, T., Shiote, M., Shoji, M., Abe, K., 2006. Intrathecal injection of epidermal growth factor and fibroblast growth factor 2 promotes proliferation of neural precursor cells in the spinal cords of mice with mutant human SOD1 gene. *J Neurosci Res.* 84, 980-92.
- Robberecht, W., 2000. Oxidative stress in amyotrophic lateral sclerosis. *J Neurol.* 247 Suppl 1, I1-6.
- Rosen, D.R., Siddique, T., Patterson, D., Figlewicz, D.A., Sapp, P., Hentati, A., Donaldson, D., Goto, J., O'Regan, J.P., Deng, H.X., et al., 1993. Mutations in Cu/Zn superoxide dismutase gene are associated with familial amyotrophic lateral sclerosis. *Nature.*

- 362, 59-62.
- Semenza, G.L., 1998. Hypoxia-inducible factor 1: master regulator of O₂ homeostasis. *Curr Opin Genet Dev.* 8, 588-94.
- Sharp, F.R., Bernaudin, M., 2004. HIF1 and oxygen sensing in the brain. *Nat Rev Neurosci.* 5, 437-48.
- Sinor, A.D., Greenberg, D.A., 2000. Erythropoietin protects cultured cortical neurons, but not astroglia, from hypoxia and AMPA toxicity. *Neurosci Lett.* 290, 213-5.
- Tanaka, T., Nangaku, M., 2009. Drug discovery for overcoming chronic kidney disease (CKD): prolyl-hydroxylase inhibitors to activate hypoxia-inducible factor (HIF) as a novel therapeutic approach in CKD. *J Pharmacol Sci.* 109, 24-31.
- Warita, H., Hayashi, T., Murakami, T., Manabe, Y., Abe, K., 2001. Oxidative damage to mitochondrial DNA in spinal motoneurons of transgenic ALS mice. *Brain Res Mol Brain Res.* 89, 147-52.
- Xu, R., Wu, C., Zhang, X., Zhang, Q., Yang, Y., Yi, J., Yang, R., Tao, Y., 2011. Linking hypoxic and oxidative insults to cell death mechanisms in models of ALS. *Brain Res.* 1372, 133-44.
- Zhang, X., Deguchi, K., Yamashita, T., Ohta, Y., Shang, J., Tian, F., Liu, N., Panin, V.L., Ikeda, Y., Matsuura, T., Abe, K., 2010. Temporal and spatial differences of multiple protein expression in the ischemic penumbra after transient MCAO in rats. *Brain Res.* 1343, 143-52.
- Zheng, C., Nennesmo, I., Fadeel, B., Henter, J.I., 2004. Vascular endothelial growth factor prolongs survival in a transgenic mouse model of ALS. *Ann Neurol.* 56, 564-7.
- Zheng, C., Skold, M.K., Li, J., Nennesmo, I., Fadeel, B., Henter, J.I., 2007. VEGF reduces astrogliosis and preserves neuromuscular junctions in ALS transgenic mice. *Biochem Biophys Res Commun.* 363, 989-93.

Figure legends

Fig. 1 - A. Nissl staining (Aa-d) and immunohistochemistry for HIF-1 α (Ae-h), VEGF (Ai-l), HO-1 (Am-p) and EPO (Aq-t) in the anterior spinal cord of wild type (WT, 18 weeks (W)) and G93A transgenic (Tg) mice at 10, 14, and 18 W. Arrowheads and arrows indicate the anterior large MNs and the surrounding glial cells, respectively, with positive protein accumulation. Scale bar = 50 μ m.

B. Quantitative analysis of HIF-1 α -, VEGF-, HO-1-, and EPO-positive MNs (Bu-1, v-1, w-1, x-1) and glial cells (Bu-2, v-2, w-2, x-2) in the anterior halves relative to the number of MNs and surrounding glial cells, respectively. The values are expressed as means \pm SD. * p < 0.05, ** p < 0.01 vs. 18W WT, ### p < 0.05, # p < 0.05 vs. 10W Tg.

Note that expression of HIF-1 α showed a progressive increase both in the anterior large MNs and surrounding glial cells in Tg mice from 14 to 18W (Af-h, Bu). The expression levels of VEGF and HO-1 also showed progressive increases but were significant only in the surrounding glial cells at 18W (Aj-l, n-p, Bv-2, w-2), while EPO was decreased in the surrounding glial cells of Tg mice at 18W (At, Bx-2).

Fig. 2 - Double immunofluorescent analysis showing HIF-1 α plus neurofilament (A), HIF-1 α plus GFAP (B), and HIF-1 α plus Iba-1 (C) in the anterior spinal cord of wild type (WT, 18W) and G93A Tg mice at 10, 14, and 18 W. Scale bars = 20 μ m. Note that HIF-1 α plus GFAP and Iba-1

double-positive surrounding glial cells showed progressive intensities at 10-18W (B, C).

Fig. 3 - Western blot analysis of HIF-1 α in the lumbar spinal cord of WT and Tg mice at 10, 14, and 18W (WT: n = 5 each; Tg: n = 5 each). Integrated density values expressed as ratios of the levels of HIF-1 α to β -tubulin. The values are expressed as means \pm SD. ** p < 0.01 vs. 18W WT, # p < 0.05, ## p < 0.01 vs. 10W Tg, § p < 0.05 vs. 14W Tg.

Fig. 4 - Western blot analysis of VEGF in the lumbar spinal cord of WT and Tg mice at 10, 14, and 18W (WT: n = 5 each; Tg: n = 5 each). Integrated density values expressed as ratios of the levels of VEGF to β -tubulin. The values are expressed as means \pm SD.

Fig. 5 - Western blot analysis of HO-1 in the lumbar spinal cord of WT and Tg mice at 10, 14, and 18W (WT: n = 5 each; Tg: n = 5 each). Integrated density values expressed as ratios of the levels of HO-1 to β -tubulin. The values are expressed as means \pm SD. ** p < 0.01 vs. 18W WT, ## p < 0.01 vs. 10W Tg.

Fig. 6 - Western blot analysis of EPO in the lumbar spinal cord of WT and Tg mice at 10, 14, and 18W (WT: n = 5 each; Tg: n = 5 each). Integrated density values expressed as ratios of the levels of EPO to β -tubulin. The values are expressed as means \pm SD.

Fig. 1

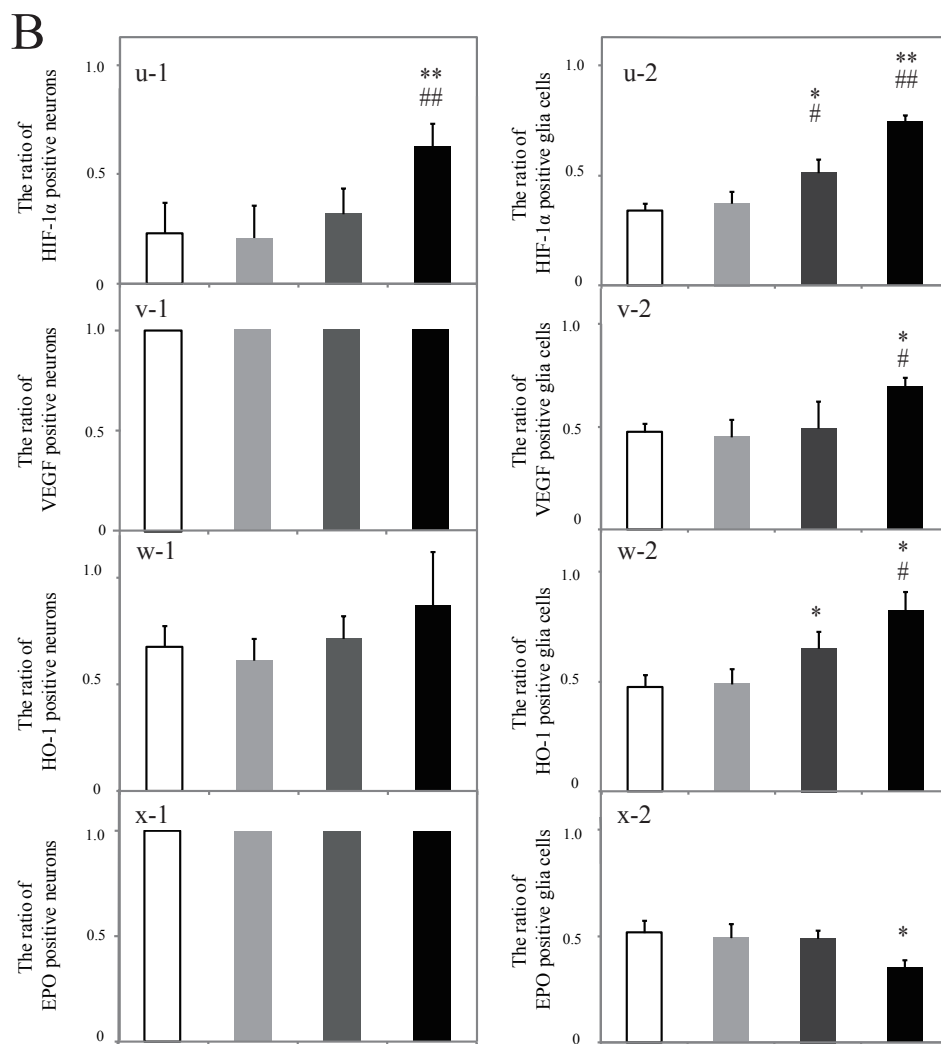
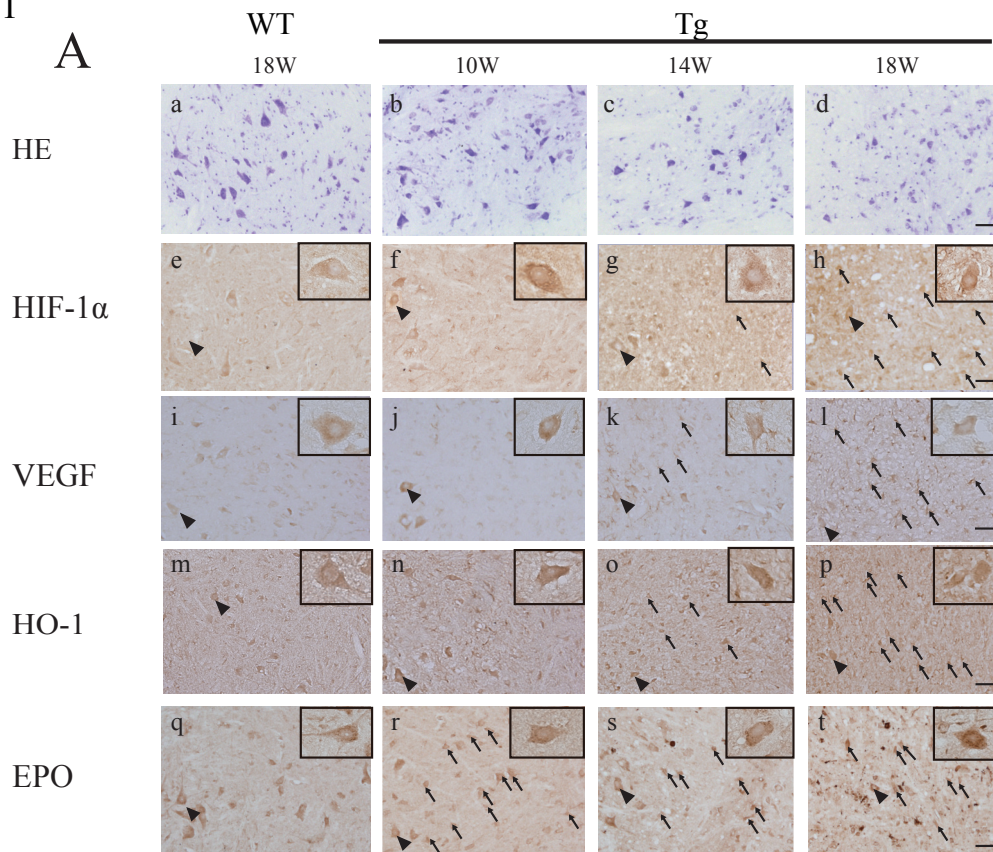


Fig. 2

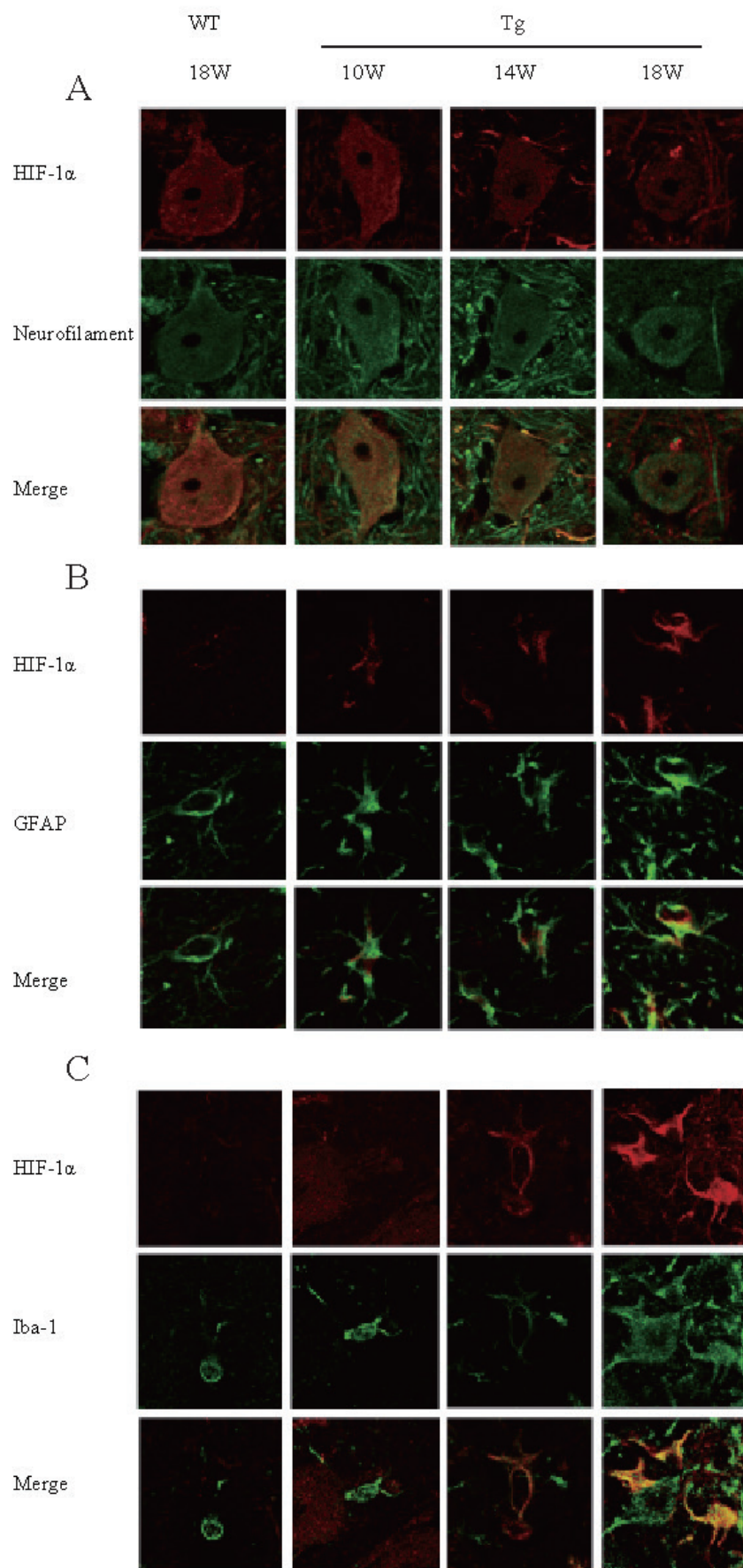


Fig. 3

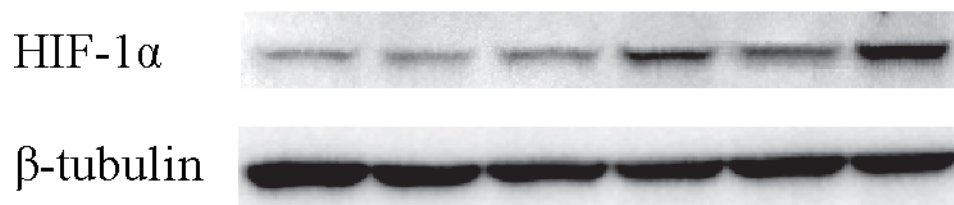
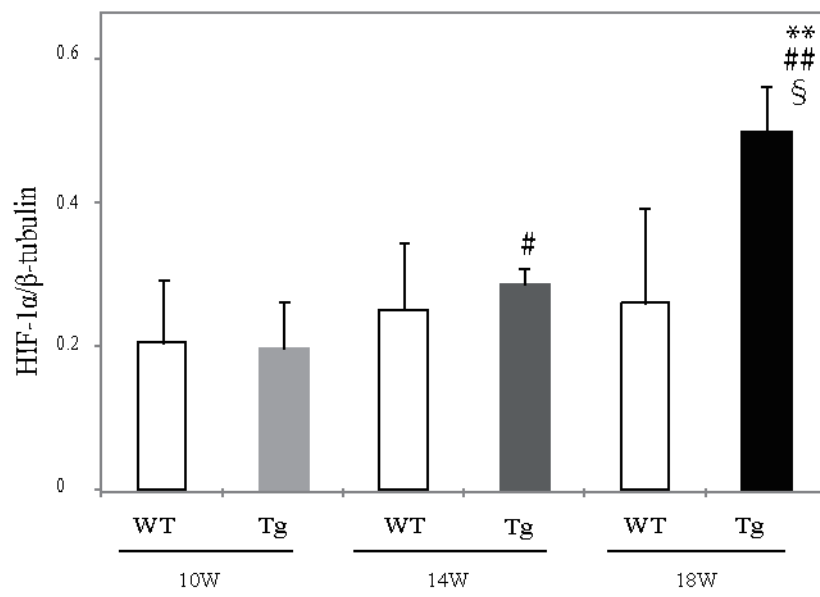
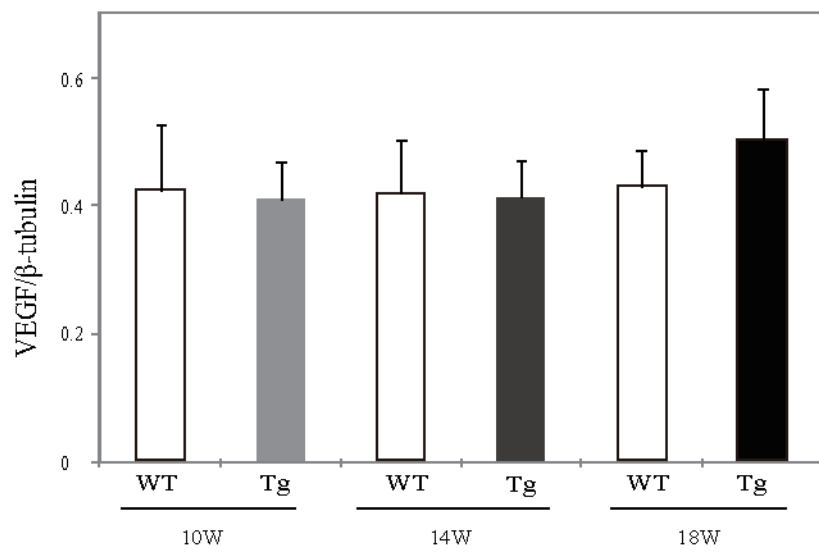


Fig. 4



VEGF



β-tubulin



Fig. 5

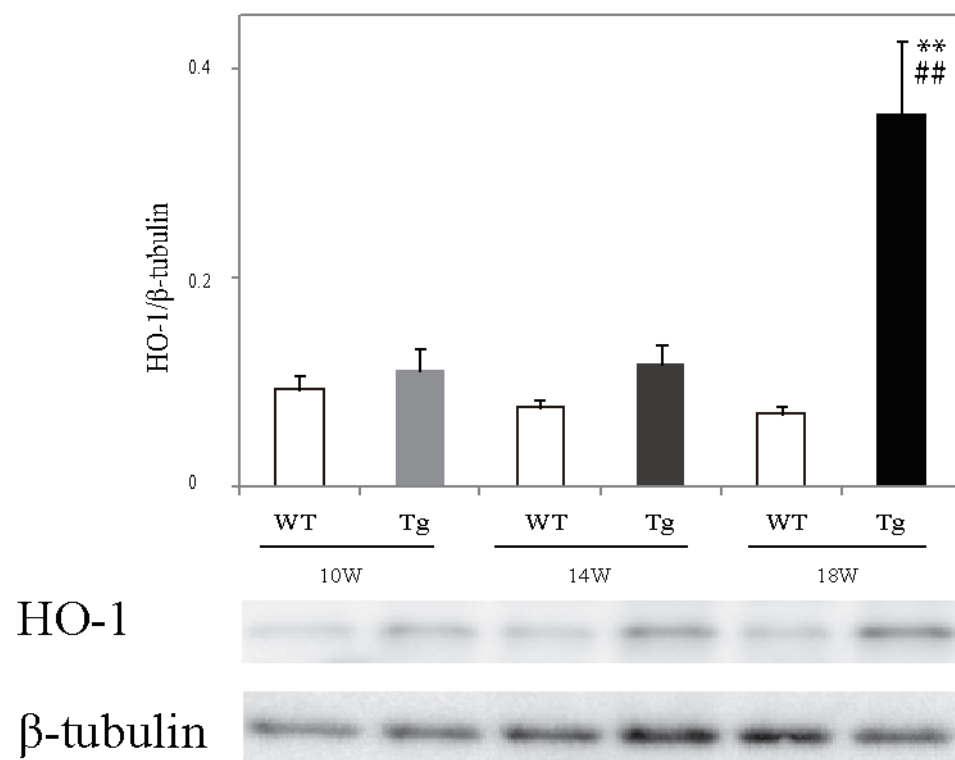


Fig. 6

